ACS APPLIED MATERIALS & INTERFACES

www.acsami.org Research Article

Rare Guest-Induced Electrical Conductivity of Zn-Porphyrin Metallacage Inclusion Complexes Featuring π-Donor/Acceptor/Donor Stacks

Paola A. Benavides, Monica A. Gordillo, Evan Thibodeaux, Ashok Yadav, Evan Johnson, Rakesh Sachdeva, and Sourav Saha*

Cite This: https://doi.org/10.1021/acsami.3c15959 Read Online

ACCESS | Metrics & More | Article Recommendations | Supporting Information

ABSTRACT: Charge-transfer (CT) interactions between co-facially aligned π-donor/acceptor (π-D/A) arrays engender unique optical and electronic properties that could benefit (supra)molecular electronics and energy technologies. Herein, we demonstrate that a tetragonal prismatic metal−organic cage ($MOC1^{8+}$) having two parallel π-donor tetrakis(4-carboxyphenyl)-Zn-porphyrin (ZnTCPP) faces selectively intercalate planar π-acceptor guests, such as hexaazatriphenylene hexacarbonitrile (HATHCN), hexacyanotriphenylene (HCTP), and napthanelediimide (NDI) derivatives, forming 1:1 πA@$MOC1^{8+}$ inclusion complexes featuring supramolecular π-D/A/D triads. The π-acidity of intercalated π-acceptors (HATHCN ≫ HCTP ≈ NDIs) dictated the nature and strength of their interactions with the ZnTCPP faces, which in turn influenced the binding affinities (K_a) and optical and electronic properties of corresponding πA@$MOC1^{8+}$ inclusion complexes. Owing to its strongest CT interaction with ZnTCPP faces, the most π-acidic HATHCN guest enjoyed the largest K_a (5×10^6 M^{-1}), competitively displaced weaker π-acceptors from the $MOC1^{8+}$ cavity, and generated the highest electrical conductivity (2.1×10^{-6} S/m) among the πA@$MOC1^{8+}$ inclusion complexes. This work demonstrates a unique through-space charge transport capability of πA@$MOC1^{8+}$ inclusion complexes featuring supramolecular π-D/A/D triads, which generated tunable electrical conductivity, which is a rare but much coveted electronic property of such supramolecular assemblies that could further expand their utility in future technologies.

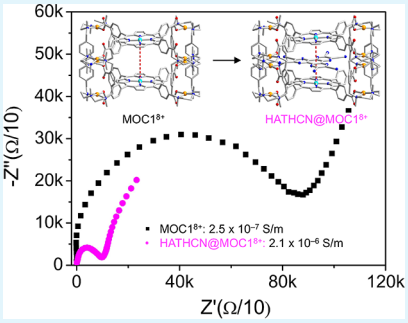

KEYWORDS: *metallacage, inclusion complex, π-donor/acceptor interaction, charge transfer, electrical conductivity*

Downloaded via CLEMSON UNIV on December 19, 2023 at 16:32:07 (UTC).
See https://pubs.acs.org/sharingguidelines for options on how to legitimately share published articles.

■ INTRODUCTION

Owing to facile through-space charge delocalization, co-facially stacked π-donor/acceptor (π-D/A) arrays[1−12] possess diverse optical and electronic properties ranging from light-harvesting,[13−21] electrochromic,[22,23] and thermochromic[24−26] behaviors to ferroelectric and semiconducting[27,28] nature that could help advance modern molecular electronics and energy technologies. Although certain combinations of strong π-donor and acceptor molecules, such as tetrathiafulvalene and tetracyanoquinodimethane, are known to form segregated homomeric π-donor and acceptor columns, which exhibit remarkable metallic conductivity due to facile intermolecular electron transfer, followed by efficient electron and hole transport through separate channels,[2,6,7] most π-donor and acceptor units only form π-D/A heterodimers[11,12,29] instead of extended alternating π-D/A stacks. Therefore, to assemble extended alternating π-D/A stacks that can potentially support long-range charge delocalization, complementary π-donor and acceptor units are usually linked covalently into π-D/A foldamers[1,30−32] or furnished with hydrogen bonding,[33−35] metal coordination sites,[36,37] or hydrophobic and amphiphilic pendants[3,38−43] that create additional stabilization through noncovalent interactions. Circumventing the need for tedious covalent modifications of π-donor and acceptor units to create extended π-D/A stacks, Fujita and co-workers[44−51] have devised an elegant template-directed Pd(II)-driven self-assembly method, which directly yielded inclusion complexes of trigonal prismatic metallacages containing extended π-D/A stacks comprising two parallel π-acidic 1,3,5-triazine faces of the cages and co-facially intercalated complementary guest π systems. While triazine-based trigonal prismatic metallacages developed by Fujita et al. typically require template-directed synthesis and directly form inclusion complexes containing intercalated templating molecules, tetragonal prismatic metallacages featuring two tetrakis(4-carboxyphenyl)-metallaporphyrin (MTCPP, M = Pd, Zn) faces connected by four bis-Pd-hexaazamacrocycle clips developed by Ribas and co-

Received: October 25, 2023
Revised: November 23, 2023
Accepted: November 29, 2023

 © XXXX American Chemical Society

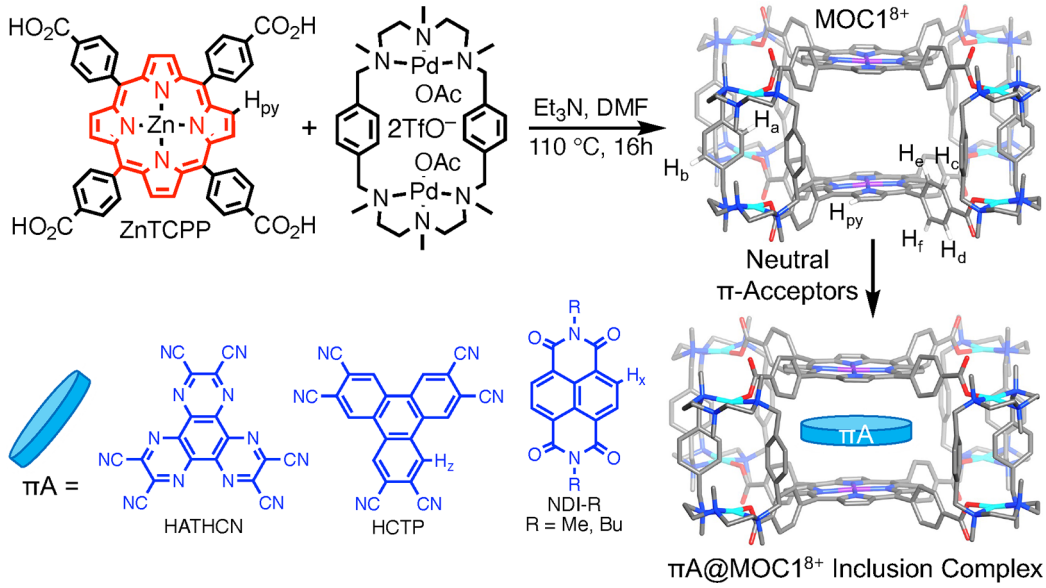

Figure 1. Formation of MOC1^{8+} and 1:1 πA@ MOC1^{8+} inclusion complexes (πA = HATHCN, HCTP, and NDIs).

workers[52−59] can be constructed without any templating guests. The height of these metallacages, that is, the distance between two opposite faces, which depends on the length of the pillar ligands, dictates the nature, number, and order of intercalated guest π systems, which in turn define their through-space charge transport capability and electronic properties. For example, a smaller metallacage with two parallel PdTCPP faces ($h \approx 7.5$ Å) encapsulated planar anionic metal-*bis*-dithiolene complexes via an electrostatic interaction but failed to sandwich any neutral π-acceptor molecules via a π-D/A charge-transfer (CT) interaction with modest π-donor PdTCPP faces,[52] whereas ZnTCPP-based larger metallacages ($h \approx 11$ Å) encapsulated electron-deficient fullerene molecules.[53,54,59] Meanwhile, we[29] and others[11] have demonstrated that Zn-porphyrins (ZnTCPP HOMO: −5.36 eV), which are stronger π-donors than Pd porphyrins (HOMO: − 5.49 eV), formed 1:1 π-D/A CT complexes with highly π-acidic neutral hexaazatriphenylene derivatives. We have further demonstrated that metal−organic frameworks (MOFs) containing extended π-D/A stacks of either mixed-valent ligands[60−62] or complementary ligands and intercalated guests[63−65] display impressive electrical conductivity due to facile through-space charge delocalization. Although the through-space charge transport capability of extended π−π and π-D/A stacks has been exploited to develop electrically conductive MOFs[66] and a wide variety of metallacages having diverse composition and architectures have been constructed in recent years,[67,68] the electrical conductivity of metallacages and their inclusion complexes containing intercalated complementary guest π systems has remained largely unexplored.[50,69] To fill this gap and realize this largely untapped potential, we envisioned that tetragonal prismatic metal−organic cages (MOCs) having two parallel electron-rich ZnTCPP faces should be able to encapsulate planar π-acceptor guests and form inclusion complexes featuring π-D/A/D stacks, which will exhibit tunable optical and electronic properties dictated by the intercalated π-acidic guests.

Herein, we demonstrate that a tetragonal prismatic metal−organic cage, namely, MOC1^{8+}·8TfO$^-$, having two parallel ZnTCPP faces located ca. 8 Å apart formed 1:1 inclusion complexes with neutral planar π-acceptors (Figure 1), such as hexaazatriphenylene hexacarbonitrile (HATHCN), hexacyanotriphenylene (HCTP), and dimethyl- and dibutyl-naphthalenediimide (NDIMe and NDIBu) derivatives with variable π-acidity and LUMO levels (HATHCN: − 4.6 eV, HCTP: − 3.7 eV, NDIMe: − 3.4 eV, and NDIBu: − 3.3 eV) but did not bind to any π-donors, such as pyrene and triphenylene (TP) due to the lack of electronic complementarity. The structures, compositions, and electronic and optical properties of MOC1^{8+} and its inclusion complexes were investigated by ^{1}H, ^{13}C, NOESY, and DOSY NMR, UV−vis, and electrochemical impedance spectroscopies (EIS). These studies demonstrated that MOC1^{8+} formed the strongest inclusion complex with the most π-acidic guest, HATHCN, which enjoyed the highest binding affinity (K_a) and competitively displaced weaker π-acceptors having lower affinities from the MOC1^{8+} cavity. The strongest ZnTCPP/HATHCN/ZnTCPP charge-transfer (CT) interaction in the HATHCN@MOC1^{8+} inclusion complex enabled the most efficient through-space charge delocalization and thereby generated the most prominent CT absorption band and the highest electrical conductivity (2.1×10^{-6} S/m).

■ RESULTS AND DISCUSSION

To exploit Zn-porphyrin's ability to form π-D/A CT complexes with neutral π-acceptors and promote through-space charge delocalization,[54−59] we synthesized tetragonal prismatic cage MOC1^{8+} by heating a solution mixture of ZnTCPP (2 equiv), a *bis*-Pd-hexaazamacrocycle clip (4 equiv), and Et_3N in DMF according to a modified literature protocol (Figure 1; also see the Supporting Information for details).[60] The structure and composition of MOC1^{8+} having two parallel ZnTCPP faces connected by four *bis*-Pd macrocyclic clips were verified by ^{1}H, COSY, and NOESY NMR (Figure S1) as well as high-resolution ESI-MS (Figure S2) analyses. The reported single-crystal structure of an isostructural metallacage having two PdTCPP faces connected by the same *bis*-Pd-hexaazamacrocycle clip revealed that the interfacial distance between the two porphyrin faces is 7.5 Å.[52] We expect that our ZnTCPP-based MOC1^{8+} should also have a similar interfacial distance,

https://doi.org/10.1021/acsami.3c15959
ACS Appl. Mater. Interfaces XXXX, XXX, XXX−XXX

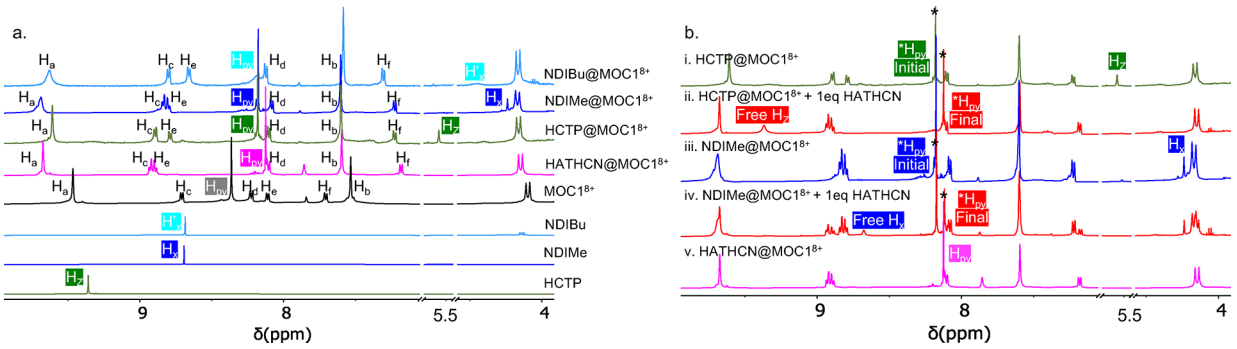

Figure 2. (a) Partial ^{1}H NMR spectra (500 MHz, CD_3CN) of empty MOC1^{8+}, free π-acceptors, and πA@MOC1^{8+} inclusion complexes show distinct upfield shifts of ZnTCPP (H_{py}) and the intercalated π-acceptors' proton signals. (b) Partial ^{1}H NMR spectra show HATHCN-induced complete displacement of HCTP (i and ii) and partial displacement of NDIMe from the MOC1^{8+} cavity (iii and iv), leading to the formation of a new HATHCN@MOC1^{8+} inclusion complex.

which is suitable for the intercalation of planar π-acceptor guests and formation of 1:1 inclusion complexes containing supramolecular π-D/A/D triads. The distinct π-donor strengths of different MTCPP (M = Pd or Zn) faces, however, should have profound effects on the electronic, optical, and molecular recognition properties of the corresponding metallacages.

We introduced four different neutral planar π-acceptors, namely, HATHCN, HCTP, *N,N′*-dimethyl-NDI (NDIMe), and *N,N′*-dibutyl-NDI (NDIBu), having distinct LUMO levels (−4.6, − 3.7, − 3.4, and −3.3 eV, respectively), which indicated their gradually diminishing π-acceptor strengths. The most π-acidic, HATHCN, formed the strongest inclusion complex with MOC1^{8+} and produced the most significant optical and electronic response compared to weaker π-acceptors. Since HATHCN does not have any trackable protons to indicate its intercalation into MOC1^{8+} by ^{1}H NMR spectroscopy, isostructural, albeit weaker, π-acidic HCTP was employed as its structural surrogate to probe this phenomenon by ^{1}H, NOESY, and DOSY NMR analysis.

The ^{1}H NMR spectra of πA@MOC1^{8+} inclusion complexes (Figure 2a) revealed that the pyrrole protons (H_{py}) of ZnTCPP faces as well as the aromatic protons of intercalated π-acceptors shifted upfield, indicating the formation of co-facially aligned π-D/A/D stacks. The intercalation of the strongest π-acceptor HATHCN between the two ZnTCPP faces of a MOC1^{8+} cage caused a larger upfield shift of the H_{py} signal (from 8.36 to 8.12 ppm, $\Delta\delta$ = 0.24 ppm) than that caused by weaker π-acidic HCTP and NDIs (from 8.36 to 8.18 ppm; $\Delta\delta$ = 0.18 ppm), revealing that the former created a stronger π-D/A/D interaction. The aromatic protons of intercalated π-acceptors underwent even greater upfield shifts—the H_z signal of HCTP shifted from 9.35 to 5.57 ppm, the H_x peak of NDIMe from 8.70 to 4.24 ppm, and H'_x of NDIBu from 8.69 to 4.44 ppm—due to the strong shielding effect of the electron-rich ZnTCPP faces of the MOC1^{8+} cage. Although the shielding of intercalated HATHCN could not be probed by ^{1}H NMR spectroscopy due to the lack of any protons, the largest upfield shift of the H_{py} signal of the MOC1^{8+} cage caused by HATHCN and the large upfield shift of H_z protons of an isostructural HCTP guest corroborated that HATHCN was also co-facially sandwiched between the ZnTCPP faces, creating an even stronger π-D/A/D interaction, which was further evident from the UV−vis spectroscopy (vide infra). The intercalation of HATHCN between two parallel ZnTCPP faces of MOC1^{8+} was further indicated by ^{13}C NMR studies (Figure S3) as the characteristic peaks of HATHCN (113.23, 135.69, and 142.43 ppm) shifted upfield in the HATHCN@MOC1^{8+} inclusion complex due to shielding by electron-rich ZnTCPP faces.

Upon the addition of 1 equiv HATHCN to preassembled HCTP@MOC1^{8+} inclusion complexes (Figure 2b-i,ii), the signature aromatic peaks of pre-intercalated HCTP (H_z at 5.57 ppm) immediately shifted downfield, returning to the original positions of free HCTP (9.35 ppm), while the H_{py} signal of ZnTCPP faces shifted further upfield (from 8.18 to 8.12 ppm), thus indicating that the stronger π-acceptor HATHCN completely displaced the weaker π-acceptor from the MOC1^{8+} cavity, forming a stronger HATHCN@MOC1^{8+} inclusion complex. On the other hand, in the presence of 1 equiv HATHCN, the ^{1}H NMR spectrum of the pre-assembled NDIMe@MOC1^{8+} inclusion complex changed more slowly as the free NDIMe signal (H_x at 8.70 ppm) appeared while the ZnTCPP H_{py} signal shifted further upfield (8.12 ppm) and reached a steady-state equilibrium after ∼3h (Figure 2b-iii,iv). Based on the integrations of distinct ZnTCPP H_{py} signals of original NDIMe@MOC1^{8+} and the newly generated HATHCN@MOC1^{8+} inclusion complexes, roughly ∼40% of the former was converted to the latter after 3 h, and this ratio remained practically unchanged after 24 h. The displacement of NDIMe was slightly faster in the presence of 2 equiv HATHCN as the steady-state equilibrium of the two inclusion complexes is reached after ∼2 h. Unlike HCTP, which was completely displaced from the MOC1^{8+} cavity by HATHCN, yielding exclusively HATHCN@MOC1^{8+} (Figure 2b-ii), NDIMe was never completely replaced by HATHCN as both inclusion complexes coexisted in a steady-state equilibrium (Figure 2b-iv). These competition experiments suggested that the strongest π-acceptor HATHCN had a much stronger binding affinity than weaker π-acidic HCTP due to a stronger π-D/A/D CT interaction with the ZnTCPP faces, which led to a fast and complete substitution; however, its advantage over another weak π-acid NDIMe appeared to be much smaller possibly due to competing desolvation/solvation effects (vide infra), which led to a slower and partial exchange. The binding affinities (K_a) of the MOC1^{8+} host and different π-acidic guests were quantified by UV−vis titration studies (vide infra). Although π-intercalated fullerene guests have been displaced from a ZnTCPP-based larger metallacage by a coordinating guest, namely, 4,4′-bipyridine, which bridged the two ZnTCPP faces via internal axial coordination,[55] our studies demonstrated for the first time that a stronger π-

https://doi.org/10.1021/acsami.3c15959
ACS Appl. Mater. Interfaces XXXX, XXX, XXX−XXX

acceptor HATHCN can also displace weaker π-acceptors from a smaller ZnTCPP-based MOC1^{8+}.

NOESY NMR analysis of πA@MOC1^{8+} inclusion complexes (Figure S4) revealed through-space coupling between H_{py} protons of ZnTCPP faces and the core protons of π-acceptors, which further verified the intercalation of π-acceptors between the ZnTCPP faces of MOC1^{8+}. In contrast, upon the addition of planar π-donor molecules, such as pyrene and TP, to MOC1^{8+}, the ^{1}H NMR spectra of neither species changed at all, confirming that they did not interact with the ZnTCPP faces (Figure S5), indicating that a complementary π-donor−acceptor interaction was vital for guest intercalation.

DOSY NMR (Figure S6, Table 1) studies further confirmed intercalation of neutral π-acceptors inside MOC1^{8+}, leading to the formation of 1:1 inclusion complexes, and ruled out the formation of 1:2 host−guest complexes having two external π-acceptors perched on the external faces of ZnTCPP panels. The diffusion coefficient of empty MOC1^{8+} ($D = 3.7 \times 10^{-10}$ m^2/s) corresponds to a hydrodynamic radius (r_H) of 16.8 Å, which is in good agreement with the reported single-crystal radius (16 Å) of an isostructural metallacage having PdTCPP faces connected by the same *bis*-Pd-metallacycle linkers.[52] On the other hand, the diffusion coefficients of planar π-acceptors ($D \approx 2.0-2.8 \times 10^{-9}$ m^2/s) are roughly an order of magnitude higher and their hydrodynamic radii were commensurately smaller (2.2−3.1 Å) than that of the 3D MOC1^{8+} cage, which has a much larger size. The diffusion coefficients and hydrodynamic radii of πA@MOC1^{8+} inclusion complexes containing intercalated HCTP and NDIMe guests ($D \approx 3.7 \times 10^{-10}$ m^2/s; r_H = 16.7−16.8 Å) are similar to those of the empty cage, indicating that these neutral π-acceptors are indeed encapsulated by the MOC1^{8+} cage. On the other hand, the HATHCN@MOC1^{8+} inclusion complex displayed considerably a higher diffusion coefficient and smaller hydrodynamic radius ($D \approx 5.5 \times 10^{-10}$ m^2/s; r_H = 11.4 Å) than the empty cage and the inclusion complexes of weaker π-acceptors, indicating that the size of MOC1^{8+} contracted upon intercalation of highly π-acidic HATHCN due to a strong π-D/A/D charge-transfer interaction, which pulled the ZnTCPP faces of MOC1^{8+} closer to the sandwiched HATHCN molecule. The HATHCN-induced contraction of the MOC1^{8+} cage was possible because the *bis*-Pd azamacrolacycle clips connecting the ZnTCPP faces are flexible enough to lend MOC1^{8+} breathing capability.

Table 1. Diffusion Coefficients (D) and Hydrodynamic Radii (r_H) of Empty MOC1^{8+}, Free π-Acceptors, and Corresponding πA@MOC1^{8+} Inclusion Complexes

compound	D (m^2/s)	r_H (Å)
HCTP	2.00×10^{-9}	3.13
NDIMe	2.82×10^{-9}	2.21
NDIBu	2.26×10^{-9}	2.75
MOC1^{8+}	3.72×10^{-10}	16.79
HCTP@MOC1^{8+}	3.72×10^{-10}	16.79
NDIMe@MOC1^{8+}	3.74×10^{-10}	16.67
HATHCN@MOC1^{8+}	5.50×10^{-10}	11.35

To gain further insight into the contraction of the HATHCN@MOC1^{8+} inclusion complex compared to empty MOC1^{8+} and HCTP@MOC1^{8+}, we calculated their energy optimized structures (Figure 3) using B3LYP/6-31g(d)/lanl2dz basis sets. The estimated distances between the two ZnTCPP faces ($d_{ZnTCPP-ZnTCPP}$) of empty MOC1^{8+}, HCTP@MOC1^{8+}, and HATHCN@MOC1^{8+} complexes are 8.03, 8.31, and 7.94 Å, respectively. These computational results confirmed that the strongest ZnTCPP/HATHCN/ZnTCPP CT interaction indeed pulled the π-donor faces of MOC1^{8+} closer to the strongest intercalated π-acceptor, while weaker π-acceptors failed to induce such a structural change due to the lack of any CT interaction (vide infra). Furthermore, in both HATHCN@MOC1^{8+} and HCTP@MOC1^{8+} complexes, the intercalated π-acceptor resided at the center of the MOC1^{8+} cavity, that is, at an equal distance from both ZnTCPP faces; however, $d_{ZnTCPP-HATHCN}$ was ca. 0.2 Å shorter than $d_{ZnTCPP-HCTP}$, indicating a stronger attractive interaction in the former.

High-resolution ESI-MS analysis (Figure 4 and Figures S7−S10) provided direct evidence of 1:1 πA@MOC1^{8+} inclusion complexes (πA = HATHCN, HCTP, NDIMe, and NDIBu) by revealing the characteristic m/z peaks with the expected isotope distribution patterns of all [πA@MOC1·8TfO − 3TfO]$^{5+}$, [πA@MOC1·8TfO − 4TfO]$^{4+}$, and [πA@MOC1·8TfO − 5TfO]$^{3+}$ species.

Having determined the structures and compositions of 1:1 πA@MOC1^{8+} inclusion complexes, we turned our attention to their electronic and optical properties. The UV−vis titration studies showed that (Figure 5a), with increasing the amount of the strongest π-acidic HATHCN, the Soret band of ZnTCPP faces of MOC1^{8+} was rapidly quenched and red-shifted from 422 to 429 nm and a new characteristic broad CT band appeared above 600 nm, which was even more prominent at a higher concentration (vide infra), revealing a strong ZnTCPP/HATHCN/ZnTCPP (π-D/A/D) CT interaction. The plot of HATHCN-induced intensity changes of the ZnTCPP Soret band as a function of their relative molar ratio (Figure 5a,

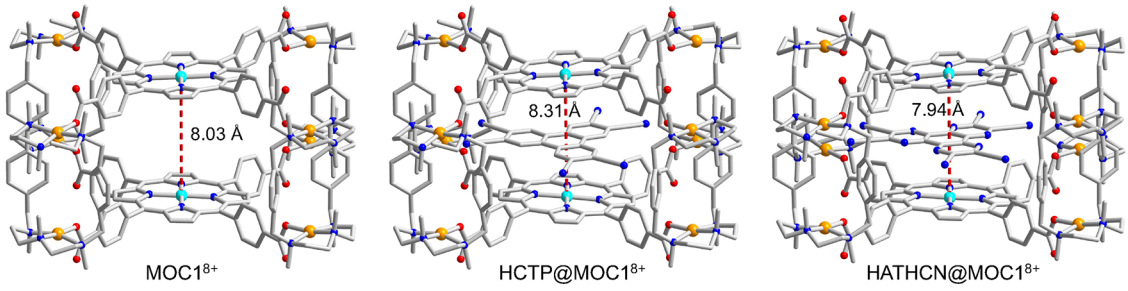

Figure 3. DFT energy-minimized structures of empty MOC1^{8+}, HCTP@MOC1^{8+}, and HATHCN@MOC1^{8+} complexes show the interfacial distances between two ZnTCPP faces ($d_{ZnTCPP-ZnTCPP}$) in all three species and indicate that it contracted in the presence of intercalated HATHCN due to a strong ZnTCPP/HATHCN/ZnTCPP CT interaction.

https://doi.org/10.1021/acsami.3c15959
ACS Appl. Mater. Interfaces XXXX, XXX, XXX−XXX

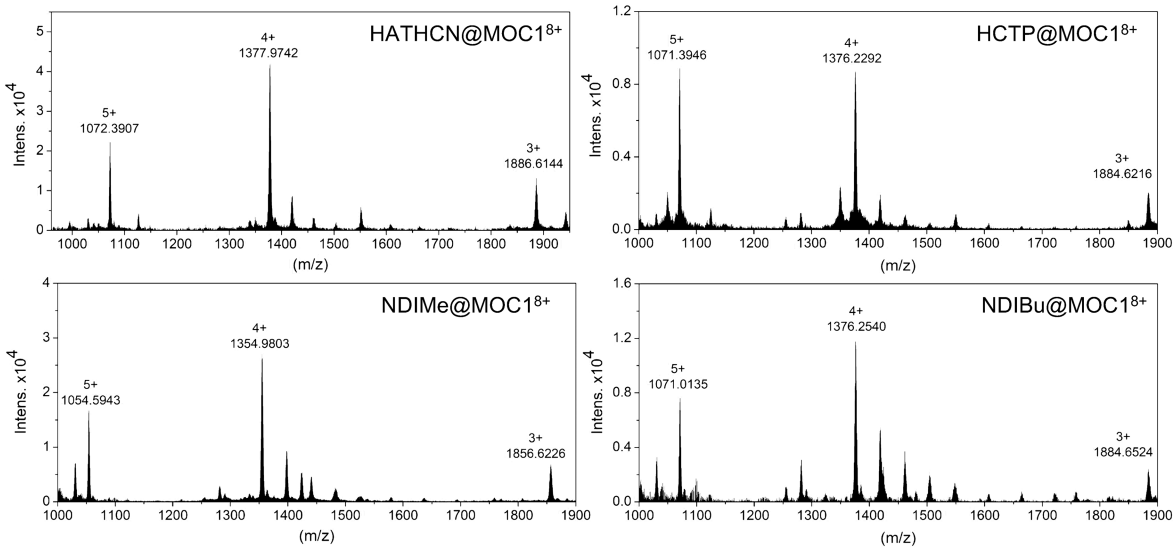

Figure 4. ESI-MS data of 1:1 πA@MOC1^{8+} inclusion complexes showing characteristic m/z signals of [πA@MOC1·8TfO − 3TfO]$^{5+}$, [πA@MOC1·8TfO − 4TfO]$^{4+}$, and [πA@MOC1·8TfO − 5TfO]$^{3+}$ species.

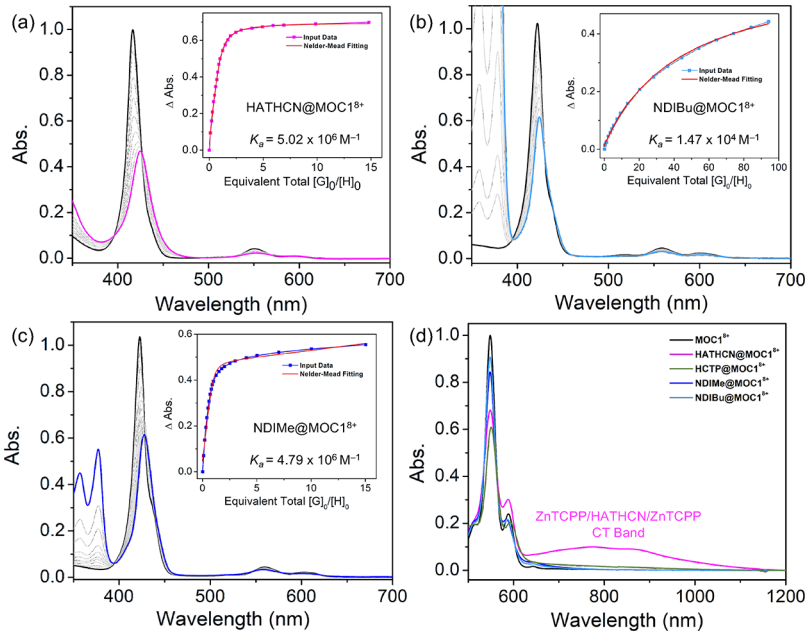

Figure 5. (a−c) UV−vis titration (inset: fitting plots) of MOC1^{8+} with (a) HATHCN, (b) NDIBu, and (c) NDIMe. (d) Final UV−vis absorption spectra of all πA@ MOC1^{8+} inclusion complexes at higher concentrations (34 μM) showing relative intensities of different π-D/A/D CT bands indicating different strengths.

inset) fit perfectly with a 1:1 binding model and revealed a large binding constant (K_a = 5.02 × 10^6 M^{-1}, 7:3 CH_2Cl_2/MeCN, 295 K). In contrast, UV−vis titration of MOC1^{8+} with a weaker π-acceptor NDIBu (Figure 5b) caused gradual quenching and a red shift of the ZnTCPP Soret band to 427 nm at a much slower rate than HATHCN (100 equiv NDIBu vs 15 equiv HATHCN was needed to reach respective saturation points), which indicated a much weaker interaction of NDIBu with the ZnTCPP faces. Consequently, NDIBu experienced 2 orders of magnitude smaller K_a (1.5 × 10^4 M^{-1}, 7:3 CH_2Cl_2/MeCN, 295 K) than HATHCN. Interestingly, the UV−vis titration of MOC1^{8+} with NDIMe (Figure 5c), which has a similar π-acidity as NDIBu, led to a faster quenching and red shift of the ZnTCPP Soret band. Accordingly, the K_a of NDIMe (4.8 × 10^6 M^{-1}, 7:3 CH_2Cl_2/MeCN, 295 K) was considerably higher than NDIBu's but slightly smaller than HATHCN's. However, unlike HATHCN, neither NDI derivatives produced any noticeable CT absorption band, indicating the lack of any significant CT interaction (Figure 5d). Since NDIBu and NDIMe have similar π-acidity (i.e., LUMO levels of −3.3 and −3.4 eV, respectively) and neither produced any noticeable CT band with the ZnTCPP faces of MOC1^{8+}, the higher K_a of the latter suggested that other factors, such as its poor solubility and weak solvent interaction (i.e., solvophobic effect), had an outsized effect on its binding, which greatly compensated for the lack of a CT interaction. Intercalation of less soluble NDIMe inside MOC1^{8+} greatly improved its solubility in the polar solvent mixture, which likely contributed to its surprisingly high K_a despite the lack of a CT interaction. On the other hand, the most π-acidic

https://doi.org/10.1021/acsami.3c15959
ACS Appl. Mater. Interfaces XXXX, XXX, XXX−XXX

HATHCN was very soluble in the same solvent system and had to shed its solvent shell in order to be intercalated inside $MOC1^{8+}$. A strong π-D/A/D CT interaction evidenced by the UV−vis spectrum helped HATHCN overcome the large desolvation penalty and register the highest K_a with $MOC1^{8+}$. Taken together, these results suggested that, while less soluble NDIMe benefited from a solvophobic effect to achieve an unusually high K_a, the most π-acidic HATHCN registered the highest K_a chiefly due to a strong CT interaction with $MOC1^{8+}$ faces, which enabled it to (partially) displace pre-intercalated NDIMe from the $MOC1^{8+}$ cavity (vide supra). In other words, two different factors—a strong π-D/A/D CT interaction for the most π-acidic HATHCN and a solvophobic effect (solvation/desolvation) for a weaker π-acidic and less soluble NDIMe—played the major role on their respective association constants.

Cyclic voltammetry (CV, Figure S11) studies revealed the electrochemical potentials (E_{ox} and E_{red}) of empty $MOC1^{8+}$, free π-acceptors, and πA@$MOC1^{8+}$ inclusion complexes and provided insight into the nature of interactions between ZnTCPP faces and intercalated π-acceptors with varying π-acidities. In the presence of the strongest π-acid HATHCN, the first oxidation (anodic) peak of ZnTCPP faces shifted by +110 mV (from +360 to +470 mV vs $E_{Fc+/Fc}$), while the first reduction (cathodic) peak of HATHCN shifted by −70 mV (from −510 to −580 mV vs $E_{Fc+/Fc}$), further confirming a strong π-D/A/D CT interaction, which rendered both donor oxidation and acceptor reduction processes more difficult. In comparison, the intercalation of less π-acidic NDIMe inside $MOC1^{8+}$, which did not produce any noticeable UV−vis CT band, had much smaller effects on the redox potentials due to insufficient CT interaction as the first anodic peak of the ZnTCPP faces and the first cathodic peak of NDIMe shifted only by +70 and −30 mV, respectively. The intercalation of NDIBu did not cause any noticeable change in the redox potentials of the ZnTCPP faces and the π-intercalator. Thus, corroborating the UV−vis data (Figure 5d), these CV results demonstrated that the strongest π-acceptor HATHCN with the lowest LUMO level ($E_{LUMO} = -4.8 - E_{red}$ eV ≈ −4.3 eV) located closest to the host metallacage's HOMO ($E_{HOMO} = -4.8 - E_{ox}$ eV ≈ −5.2 eV) enjoyed a significant CT interaction, while the weaker π-acidic NDI derivatives with much higher LUMO levels ($E_{LUMO} = -4.8 - E_{red}$ eV ≈ −3.3 eV) failed to do so.

Finally, we studied the effects of intercalation of the strongest (HATHCN) and weakest (NDIBu) π-acceptors on the electronic properties of the corresponding inclusion complexes. For this, we measured the electrical conductivity of drop-cast films of empty $MOC1^{8+}$, HATHCN@$MOC1^{8+}$, and NDIBu@$MOC1^{8+}$ complexes deposited on interdigitated Au electrodes on nonconductive glass surfaces by electrochemical impedance spectroscopy (EIS). The Nyquist plots of (Figure 6) revealed that, compared to empty $MOC1^{8+}$, both inclusion complexes enjoyed a much smaller charge transfer resistance (i.e., smaller semicircles), which corresponded to an order of magnitude higher electrical conductivity for HATHCN@$MOC1^{8+}$ (2.1×10^{-6} S/m) and NDIBu@$MOC1^{8+}$ (1.2×10^{-6} S/m) than the empty $MOC1^{8+}$ (2.5×10^{-7} S/m). The conductivity of HATHCN@$MOC1^{8+}$ was roughly double that of NDIBu@$MOC1^{8+}$, indicating that the stronger guest-mediated π-D/A/D CT interaction in the former facilitated a more efficient charge delocalization. These results demonstrated that the most π-acidic HATHCN with the lowest LUMO level, which created the strongest π-D/A/D CT interaction with the ZnTCPP faces of the $MOC1^{8+}$ cage, also generated the highest electrical conductivity by enabling the most efficient through-space charge delocalization.

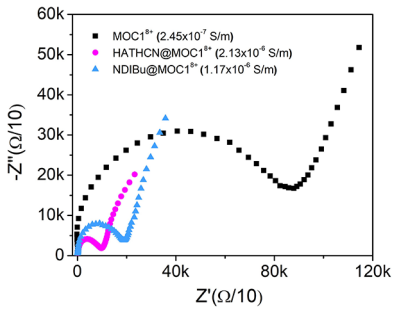

Figure 6. Nyquist plots of empty $MOC1^{8+}$, HATHCN@$MOC1^{8+}$, and NDIMe@$MOC1^{8+}$ inclusion complexes reveal their respective charge transfer resistances and electrical conductivity.

CONCLUSIONS

In summary, we have synthesized a new ZnTCPP-based tetragonal prismatic $MOC1^{8+}$ via a template-free Pd(II)-driven self-assembly protocol. Unlike an analogous metallacage having weaker π-donor PdTCPP faces, which encapsulated only planar anionic metal−dithiolene complexes via electrostatic interactions but did not create any π-D/A/D CT interaction, the stronger π-donor ZnTCPP-based $MOC1^{8+}$ faces selectively encapsulated neutral planar π-acceptors, forming 1:1 πA@$MOC1^{8+}$ inclusion complexes. The strength of the π-acceptors indicated by their respective LUMO levels dictated the strength of ZnTCPP/πA/ZnTCPP interactions, which in turn defined the guest binding affinity, selectivity, efficacy of through-space charge delocalization, and thus the optical and electronic properties of the resulting πA@$MOC1^{8+}$ complexes. The strongest π-acceptor HATHCN, which enjoyed the strongest π-D/A/D CT interaction with the ZnTCPP faces as evident from the most prominent CT band, not only displaced the weaker π-acceptors from the $MOC1^{8+}$ cavity but also generated the highest electrical conductivity in the resulting HATHCN@$MOC1^{8+}$ inclusion complex. Although π-donor/acceptor and π−π interactions have been widely exploited for guest encapsulation, separation, and sensing applications, this study presents a rare example where supramolecular π-D/A/D triads formed by intercalation of complementary planar π-acceptors inside a ZnTCPP-based metallacage facilitated through-space charge delocalization, thus creating a higher electrical conductivity. This work paves the way for employing ZnTCPP-based larger metallacages to encapsulate multiple complementary guests and create more elongated π-D/A arrays that can serve as electrically conductive supramolecular wires by facilitating though-space charge delocalization over longer distances—a tantalizing possibility, which is currently under investigation in our laboratory.

ASSOCIATED CONTENT

Supporting Information

The Supporting Information is available free of charge at https://pubs.acs.org/doi/10.1021/acsami.3c15959.

Additional experimental details, materials and methods, NMR, ESI-MS, and CV data (PDF)

https://doi.org/10.1021/acsami.3c15959
ACS Appl. Mater. Interfaces XXXX, XXX, XXX−XXX

AUTHOR INFORMATION

Corresponding Author

Sourav Saha − *Department of Chemistry, Clemson University, Clemson, South Carolina 29634, United States;* orcid.org/0000-0001-6610-4820; Email: souravs@clemson.edu

Authors

Paola A. Benavides − *Department of Chemistry, Clemson University, Clemson, South Carolina 29634, United States*

Monica A. Gordillo − *Department of Chemistry, Clemson University, Clemson, South Carolina 29634, United States*

Evan Thibodeaux − *Department of Chemistry, Clemson University, Clemson, South Carolina 29634, United States*

Ashok Yadav − *Department of Chemistry, Clemson University, Clemson, South Carolina 29634, United States*

Evan Johnson − *Department of Chemistry, Clemson University, Clemson, South Carolina 29634, United States*

Rakesh Sachdeva − *Department of Chemistry, Clemson University, Clemson, South Carolina 29634, United States*

Complete contact information is available at: https://pubs.acs.org/10.1021/acsami.3c15959

Author Contributions

The manuscript was written through contributions of all authors. All authors approved the final version of the manuscript.

Notes

The authors declare no competing financial interest.

ACKNOWLEDGMENTS

This work was supported by the US National Science Foundation (award nos. CHE-2203985, DMR-1809092, and DMR-2321365). We also acknowledge grant no. NSF-MRI-1725919 for a 500 MHz NMR instrument with a cryoprobe, which was used for certain NMR experiments.

REFERENCES

(1) Scott Lokey, R.; Iverson, B. L. Synthetic Molecules That Fold into a Pleated Secondary Structure in Solution. *Nature* **1995**, *375*, 303−305.

(2) Ferraris, J.; Cowan, D. O.; Walatka, V.; Perlstein, J. H. Electron Transfer in a New Highly Conducting Donor-Acceptor Complex. *J. Am. Chem. Soc.* **1973**, *95*, 948−949.

(3) Kumar, M.; Venkata Rao, K.; George, S. J. Supramolecular Charge Transfer Nanostructures. *Phys. Chem. Chem. Phys.* **2014**, *16*, 1300−1313.

(4) Klosterman, J. K.; Fujita, M.; Yamauchi, Y. Engineering Discrete Stacks of Aromatic Molecules. *Chem. Soc. Rev.* **2009**, *38*, 1714−1725.

(5) Das, A.; Ghosh, S. Supramolecular Assemblies by Charge-Transfer Interactions between Donor and Acceptor Chromophores. *Angew. Chem., Int. Ed.* **2014**, *53*, 2038−2054.

(6) Jérome, D. Organic Conductors: From Charge Density Wave TTF-TCNQ to Superconducting $(TMTSF)_2PF_6$. *Chem. Rev.* **2004**, *104*, 5565−5591.

(7) Alves, H.; Molinari, A. S.; Xie, H.; Morpurgo, A. F. Metallic Conduction at Organic Charge-Transfer Interfaces. *Nat. Mater.* **2008**, *7*, 574−580.

(8) Hayes, W.; Greenland, B. W. Donor−Acceptor π−π Stacking Interactions: From Small Molecule Complexes to Healable Supramolecular Polymer Networks. *Adv. Polym. Sci.* **2015**, *268*, 143−166.

(9) Zhang, J.; Xu, W.; Sheng, P.; Zhao, G.; Zhu, D. Organic Donor-Acceptor Complexes as Novel Organic Semiconductors. *Acc. Chem. Res.* **2017**, *50*, 1654−1662.

(10) Venkataraman, D.; Yurt, S.; Venkatraman, B. H.; Gavvalapalli, N. Role of Molecular Architecture in Organic Photovoltaic Cells. *J. Phys. Chem. Lett.* **2010**, *1*, 947−958.

(11) Aoki, T.; Sakai, H.; Ohkubo, K.; Sakanoue, T.; Takenobu, T.; Fukuzumi, S.; Hasobe, T. Ultrafast Photoinduced Electron Transfer in Face-to-Face Charge-Transfer π-Complexes of Planar Porphyrins and Hexaazatriphenylene Derivatives. *Chem. Sci.* **2015**, *6*, 1498−1509.

(12) Klivansky, L. M.; Hanifi, D.; Koshkakaryan, G.; Holycross, D. R.; Gorski, E. K.; Wu, Q.; Chai, M.; Liu, Y. A Complementary Disk-Shaped π Electron Donor−Acceptor Pair with High Binding Affinity. *Chem. Sci.* **2012**, *3*, 2009−2014.

(13) D'Souza, F.; Smith, P. M.; Zandler, M. E.; McCarty, A. L.; Itou, M.; Araki, Y.; Ito, O. Energy Transfer Followed by Electron Transfer in a Supramolecular Triad Composed of Boron Dipyrrin, Zinc Porphyrin, and Fullerene: A Model for the Photosynthetic Antenna-Reaction Center Complex. *J. Am. Chem. Soc.* **2004**, *126*, 7898−7907.

(14) Maligaspe, E.; Sandanayaka, A. S. D.; Hasobe, T.; Ito, O.; D'Souza, F. Sensitive Efficiency of Photoinduced Electron Transfer to Band Gaps of Semiconductive Single-Walled Carbon Nanotubes with Supramolecularly Attached Zinc Porphyrin Bearing Pyrene Glues. *J. Am. Chem. Soc.* **2010**, *132*, 8158−8164.

(15) Subbaiyan, N. K.; Hill, J. P.; Ariga, K.; Fukuzumi, S.; D'souza, F. Enhanced Photocurrents via Redox Modulation by Fluoride Binding to Oxoporphyrinogen in a Zinc Porphyrin-Oxoporphyrinogen Surface Modified TiO2 Supramolecular Solar Cell. *Chem. Commun.* **2011**, *47*, 6003−6005.

(16) Panda, D. K.; Goodson, F. S.; Ray, S.; Lowell, R.; Saha, S. Multichromophoric Dye-Sensitized Solar Cells Based on Supramolecular Zinc-Porphyrin···perylene-Imide Dyads. *Chem. Commun.* **2012**, *48*, 8775−8777.

(17) Panda, D. K.; Goodson, F. S.; Ray, S.; Saha, S. Dye-Sensitized Solar Cells Based on Multichromophoric Supramolecular Light-Harvesting Materials. *Chem. Commun.* **2014**, *50*, 5358−5360.

(18) Gust, D.; Moore, T. A.; Moore, A. L. Mimicking Photosynthetic Solar Energy Transduction. *Acc. Chem. Res.* **2001**, *34*, 40−48.

(19) Imahori, H. Giant Multiporphyrin Arrays as Artificial Light-Harvesting Antennas. *J. Phys. Chem. B* **2004**, *108*, 6130−6143.

(20) Saha, S.; Johansson, E.; Flood, A. H.; Tseng, H.-R.; Zink, J. I.; Stoddart, J. F. A Photoactive Molecular Triad as a Nanoscale Power Supply for a Supramolecular Machine. *Chem. - Eur. J.* **2005**, *11*, 6846−6858.

(21) Kelber, J. B.; Panjwani, N. A.; Wu, D.; Gómez-Bombarelli, R.; Lovett, B. W.; Morton, J. J. L.; Anderson, H. L. Synthesis and Investigation of Donor-Porphyrin-Acceptor Triads with Long-Lived Photo-Induced Charge-Separate States. *Chem. Sci.* **2015**, *6*, 6468−6481.

(22) Lv, X.; Li, W.; Ouyang, M.; Zhang, Y.; Wright, D. S.; Zhang, C. Polymeric Electrochromic Materials with Donor-Acceptor Structures. *J. Mater. Chem. C* **2017**, *5*, 12−28.

(23) Huang, J. J.; Lin, H. A.; Chen, C.; Tang, P. W.; Luo, S. C. Corannulene-Based Donor-Acceptor-Type Conjugated Polymers with Electrochromic Properties. *J. Mater. Chem. C* **2021**, *9*, 7919−7927.

(24) Alvey, P. M.; Reczek, J. J.; Lynch, V.; Iverson, B. L. A Systematic Study of Thermochromic Aromatic Donor-Acceptor Materials. *J. Org. Chem.* **2010**, *75*, 7682−7690.

(25) Peebles, C.; Wight, C. D.; Iverson, B. L. Solution- and Solid-State Photophysical and Stimuli-Responsive Behavior in Conjugated Monoalkoxynaphthalene-Naphthalimide Donor-Acceptor Dyads. *J. Mater. Chem. C* **2015**, *3*, 12156−12163.

(26) Wang, T.; Hu, Z.; Nie, X.; Huang, L.; Hui, M.; Sun, X.; Zhang, G. Thermochromic Aggregation-Induced Dual Phosphorescence via Temperature-Dependent sp^3-Linked Donor-Acceptor Electronic Coupling. *Nat. Commun.* **2021**, *12* (1), 1364.

(27) Tayi, A. S.; Shveyd, A. K.; Sue, A. C.-H.; Szarko, J. M.; Rolczynski, B. S.; Cao, D.; Kennedy, T. J.; Sarjeant, A. A.; Stern, C. L.; Paxton, W. F.; Wu, W.; Dey, S. K.; Fahrenbach, A. C.; Guest, J. R.; Mohseni, H.; Chen, L. X.; Wang, K. L.; Stoddart, J. F.; Stupp, S. I.

Room-Temperature Ferroelectricity in Supramolecular Networks of Charge-Transfer Complexes. *Nature* **2012**, *488*, 485−489.
(28) Park, S. K.; Varghese, S.; Kim, J. H.; Yoon, S. J.; Kwon, O. K.; An, B. K.; Gierschner, J.; Park, S. Y. Tailor-Made Highly Luminescent and Ambipolar Transporting Organic Mixed Stacked Charge-Transfer Crystals: An Isometric Donor-Acceptor Approach. *J. Am. Chem. Soc.* **2013**, *135*, 4757−4764.
(29) Benavides, P. A.; Gordillo, M. A.; Yadav, A.; Joaqui-Joaqui, M. A.; Saha, S. Pt(II)-Coordinated Tricomponent Self-Assemblies of Tetrapyridyl Porphyrin and Dicarboxylate Ligands: Are They 3D Prisms or 2D Bow-Ties? *Chem. Sci.* **2022**, *13*, 4070−4081.
(30) Gabriel, G. J.; Iverson, B. L. Aromatic Oligomers That Form Hetero Duplexes in Aqueous Solution. *J. Am. Chem. Soc.* **2002**, *124*, 15174−15175.
(31) Wolffs, M.; Delsuc, N.; Veldman, D.; Anh, N. V.; Williams, R. M.; Meskers, S. C. J.; Janssen, R. A. J.; Huc, I.; Schenning, A. P. H. J. Helical Aromatic Oligoamide Foldamers as Organizational Scaffolds for Photoinduced Charge Transfer. *J. Am. Chem. Soc.* **2009**, *131*, 4819−4829.
(32) Yuan, D.; Awais, M. A.; Sharapov, V.; Liu, X.; Neshchadin, A.; Chen, W.; Bera, M.; Yu, L. Foldable Semi-Ladder Polymers: Novel Aggregation Behavior and High-Performance Solution-Processed Organic Light-Emitting Transistors. *Chem. Sci.* **2020**, *11*, 11315−11321.
(33) Mukhopadhyay, P.; Iwashita, Y.; Shirakawa, M.; Kawano, S.; Fujita, N.; Shinkai, S. Spontaneous Colorimetric Sensing of the Positional Isomers of Dihydroxynaphthalene in a 1D Organogel Matrix. *Angew. Chem., Int. Ed.* **2006**, *45*, 1592−1595.
(34) Molla, M. R.; Ghosh, S. Hydrogen-Bonding-Mediated Vesicular Assembly of Functionalized Naphthalene−Diimide-Based Bolaamphiphile and Guest-Induced Gelation in Water. *Chem. - Eur. J.* **2012**, *18*, 9860−9869.
(35) Mukherjee, A.; Barman, S.; Ghosh, A.; Datta, A.; Datta, A.; Ghosh, S. A Hierarchical (Macro)Molecular Assembly Assisted by Donor−Acceptor Charge-Transfer Interactions Exhibiting Room-Temperature Ferroelectricity. *Angew. Chem., Int. Ed.* **2022**, *61*, No. e202203817.
(36) Ghosh, S.; Ramakrishnan, S. Aromatic Donor−Acceptor Charge-Transfer and Metal-Ion-Complexation-Assisted Folding of a Synthetic Polymer. *Angew. Chem.* **2004**, *116*, 3326−3330.
(37) Ghosh, S.; Ramakrishnan, S. Structural Fine-Tuning of (-Donor-Spacer-Acceptor-Spacer-)n Type Foldamers. Effect of Spacer Segment Length, Temperature, and Metal-Ion Complexation on the Folding Process. *Macromolecules* **2005**, *38*, 676−686.
(38) Wang, C.; Wang, Z.; Zhang, X. Amphiphilic Building Blocks for Self-Assembly: From Amphiphiles to Supra-Amphiphiles. *Acc. Chem. Res.* **2012**, *45*, 608−618.
(39) Sagade, C. A.; Rao, K. V.; Mogera, U.; George, S. J.; Datta, A.; Kulkarni, G. U. High-Mobility Field Effect Transistors Based on Supramolecular Charge Transfer Nanofibres. *Adv. Mater.* **2013**, *25*, 559−564.
(40) Sagade, A. A.; Rao, K. V.; George, S. J.; Datta, A.; Kulkarni, G. U. A Charge Transfer Single Crystal Field Effect Transistor Operating at Low Voltages. *Chem. Commun.* **2013**, *49*, 5847−5849.
(41) Rao, K. V.; George, S. J. Supramolecular Alternate Co-Assembly through a Non-Covalent Amphiphilic Design: Conducting Nanotubes with a Mixed D−A Structure. *Chem. - Eur. J.* **2012**, *18*, 14286−14291.
(42) Liu, K.; Wang, C.; Li, Z.; Zhang, X. Superamphiphiles Based on Directional Charge-Transfer Interactions: From Supramolecular Engineering to Well-Defined Nanostructures. *Angew. Chem.* **2011**, *123*, 5054−5058.
(43) Wang, C.; Yin, S.; Chen, S.; Xu, H.; Wang, Z.; Zhang, X. Controlled Self-Assembly Manipulated by Charge-Transfer Interactions: From Tubes to Vesicles. *Angew. Chem., Int. Ed.* **2008**, *47*, 9049−9052.
(44) Kumazawa, K.; Biradha, K.; Kusukawa, T.; Okano, T.; Fujita, M. Multicomponent Assembly of a Pyrazine-Pillared Coordination Cage That Selectively Binds Planar Guests by Intercalation. *Angew. Chem., Int. Ed.* **2003**, *42*, 3909−3913.
(45) Yoshizawa, M.; Nakagawa, J.; Kumazawa, K.; Nagao, M.; Kawano, M.; Ozeki, T.; Fujita, M. Discrete Stacking of Large Aromatic Molecules within Organic-Pillared Coordination Cages. *Angew. Chem., Int. Ed.* **2005**, *44*, 1810−1813.
(46) Yoshizawa, M.; Kumazawa, K.; Fujita, M. Room-Temperature and Solution-State Observation of the Mixed-Valence Cation Radical Dimer of Tetrathiafulvalene, $[(TTF)_2]^{+\cdot}$, within a Self-Assembled Cage. *J. Am. Chem. Soc.* **2005**, *127*, 13456−13457.
(47) Ono, K.; Yoshizawa, M.; Kato, T.; Watanabe, K.; Fujita, M. Porphine Dimeric Assemblies in Organic-Pillared Coordination Cages. *Angew. Chem., Int. Ed.* **2007**, *46*, 1803−1806.
(48) Yamauchi, Y.; Yoshizawa, M.; Akita, M.; Fujita, M. Engineering Double to Quintuple Stacks of a Polarized Aromatic in Confined Cavities. *J. Am. Chem. Soc.* **2010**, *132*, 960−966.
(49) Murase, T.; Otsuka, K.; Fujita, M. Pairwise Selective Formation of Aromatic Stacks in a Coordination Cage. *J. Am. Chem. Soc.* **2010**, *132*, 7864−7865.
(50) Fujii, S.; Tada, T.; Komoto, Y.; Osuga, T.; Murase, T.; Fujita, M.; Kiguchi, M. Rectifying Electron-Transport Properties through Stacks of Aromatic Molecules Inserted into a Self-Assembled Cage. *J. Am. Chem. Soc.* **2015**, *137*, 5939−5947.
(51) Iwane, M.; Tada, T.; Osuga, T.; Murase, T.; Fujita, M.; Nishino, T.; Kiguchi, M.; Fujii, S. Controlling Stacking Order and Charge Transport in π-Stacks of Aromatic Molecules Based on Surface Assembly. *Chem. Commun.* **2018**, *54*, 12443−12446.
(52) García-Simón, C.; Garcia-Borràs, M.; Gómez, L.; Garcia-Bosch, I.; Osuna, S.; Swart, M.; Luis, J. M.; Rovira, C.; Almeida, M.; Imaz, I.; Maspoch, D.; Costas, M.; Ribas, X. Self-Assembled Tetragonal Prismatic Molecular Cage Highly Selective for Anionic π Guests. *Chem. - Eur. J.* **2013**, *19*, 1445−1456.
(53) García-Simón, C.; Garcia-Borràs, M.; Gómez, L.; Parella, T.; Osuna, S.; Juanhuix, J.; Imaz, I.; Maspoch, D.; Costas, M.; Ribas, X. Sponge-like Molecular Cage for Purification of Fullerenes. *Nat. Commun.* **2014**, *5*, 5557.
(54) Colomban, C.; Szalóki, G.; Allain, M.; Gómez, L.; Goeb, S.; Sallé, M.; Costas, M.; Ribas, X. Reversible C60 Ejection from a Metallocage through the Redox-Dependent Binding of a Competitive Guest. *Chem. - Eur. J.* **2017**, *23*, 3016−3022.
(55) Colomban, C.; Martin-Diaconescu, V.; Parella, T.; Goeb, S.; García-Simón, C.; Lloret-Fillol, J.; Costas, M.; Ribas, X. Design of Zn-, Cu-, and Fe-Coordination Complexes Confined in a Self-Assembled Nanocage. *Inorg. Chem.* **2018**, *57*, 3529−3539.
(56) Fuertes-Espinosa, C.; Gómez-Torres, A.; Morales-Martínez, R.; Rodríguez-Fortea, A.; García-Simón, C.; Gándara, F.; Imaz, I.; Juanhuix, J.; Maspoch, D.; Poblet, J. M.; Echegoyen, L.; Ribas, X. Purification of Uranium-Based Endohedral Metallofullerenes (EMFs) by Selective Supramolecular Encapsulation and Release. *Angew. Chem., Int. Ed.* **2018**, *57*, 11294−11299.
(57) Colomban, C.; Fuertes-Espinosa, C.; Goeb, S.; Sallé, M.; Costas, M.; Blancafort, L.; Ribas, X. Self-Assembled Cofacial Zinc−Porphyrin Supramolecular Nanocapsules as Tuneable 1O2 Photosensitizers. *Chem. - Eur. J.* **2018**, *24*, 4371−4381.
(58) García-Simón, C.; Monferrer, A.; Garcia-Borràs, M.; Imaz, I.; Maspoch, D.; Costas, M.; Ribas, X. Size-Selective Encapsulation of C60 and C60-Derivatives within an Adaptable Naphthalene-Based Tetragonal Prismatic Supramolecular Nanocapsule. *Chem. Commun.* **2019**, *55*, 798−801.
(59) Ubasart, E.; Borodin, O.; Fuertes-Espinosa, C.; Xu, Y.; García-Simón, C.; Gómez, L.; Juanhuix, J.; Gándara, F.; Imaz, I.; Maspoch, D.; von Delius, M.; Ribas, X. A Three-Shell Supramolecular Complex Enables the Symmetry-Mismatched Chemo- and Regioselective Bis-Functionalization of C_{60}. *Nat. Chem.* **2021**, *13*, 420−427.
(60) Gordillo, M. A.; Benavides, P. A.; Panda, D. K.; Saha, S. The Advent of Electrically Conducting Double-Helical Metal-Organic Frameworks Featuring Butterfly-Shaped Electron-Rich π-Extended Tetrathiafulvalene Ligands. *ACS Appl. Mater. Interfaces* **2020**, *12*, 12955−12961.

https://doi.org/10.1021/acsami.3c15959
ACS Appl. Mater. Interfaces XXXX, XXX, XXX−XXX

(61) Gordillo, M. A.; Benavides, P. A.; Spalding, K.; Saha, S. A New Electrically Conducting Metal−Organic Framework Featuring U-Shaped Cis-Dipyridyl Tetrathiafulvalene Ligands. *Front. Chem.* **2021**, *9* (792), No. 726544.
(62) Zhang, S.; Panda, D. K.; Yadav, A.; Zhou, W.; Saha, S. Effects of Intervalence Charge Transfer Interaction between π-Stacked Mixed Valent Tetrathiafulvalene Ligands on the Electrical Conductivity of 3D Metal-Organic Frameworks. *Chem. Sci.* **2021**, *12*, 13379−13391.
(63) Guo, Z.; Panda, D. K.; Gordillo, M. A.; Khatun, A.; Wu, H.; Zhou, W.; Saha, S. Lowering Band Gap of an Electroactive Metal-Organic Framework via Complementary Guest Intercalation. *ACS Appl. Mater. Interfaces* **2017**, *9*, 32413−32417.
(64) Yadav, A.; Zhang, S.; Benavides, P. A.; Zhou, W.; Saha, S. Electrically Conductive π-Intercalated Graphitic Metal-Organic Framework Containing Alternate π-Donor/Acceptor Stacks. *Angew. Chem., Int. Ed.* **2023**, *62*, No. e202303819.
(65) Guo, Z.; Panda, D. K.; Maity, K.; Lindsey, D.; Parker, T. G.; Albrecht-Schmitt, T. E.; Barreda-Esparza, J. L.; Xiong, P.; Zhou, W.; Saha, S. Modulating the Electrical Conductivity of Metal-Organic Framework Films with Intercalated Guest π-Systems. *J. Mater. Chem. C* **2016**, *4*, 894−899.
(66) Xie, L. S.; Skorupskii, G.; Dincă, M. Electrically Conductive Metal−Organic Frameworks. *Chem. Rev.* **2020**, *120*, 8536−8580.
(67) McTernan, C. T.; Davies, J. A.; Nitschke, J. R. Beyond Platonic: How to Build Metal−Organic Polyhedra Capable of Binding Low-Symmetry. *Information-Rich Molecular Cargoes. Chem. Rev.* **2022**, *122*, 10393−10437.
(68) Saha, R.; Mondal, B.; Mukherjee, P. S. Molecular Cavity for Catalysis and Formation of Metal Nanoparticles for Use in Catalysis. *Chem. Rev.* **2022**, *122*, 12244−12307.
(69) Kiguchi, M.; Takahashi, T.; Takahashi, Y.; Yamauchi, Y.; Murase, T.; Fujita, M.; Tada, T.; Watanabe, S. Electron Transport through Single Molecules Comprising Aromatic Stacks Enclosed in Self-Assembled Cages. *Angew. Chem., Int. Ed.* **2011**, *50*, 5708−5711.

https://doi.org/10.1021/acsami.3c15959
ACS Appl. Mater. Interfaces XXXX, XXX, XXX−XXX